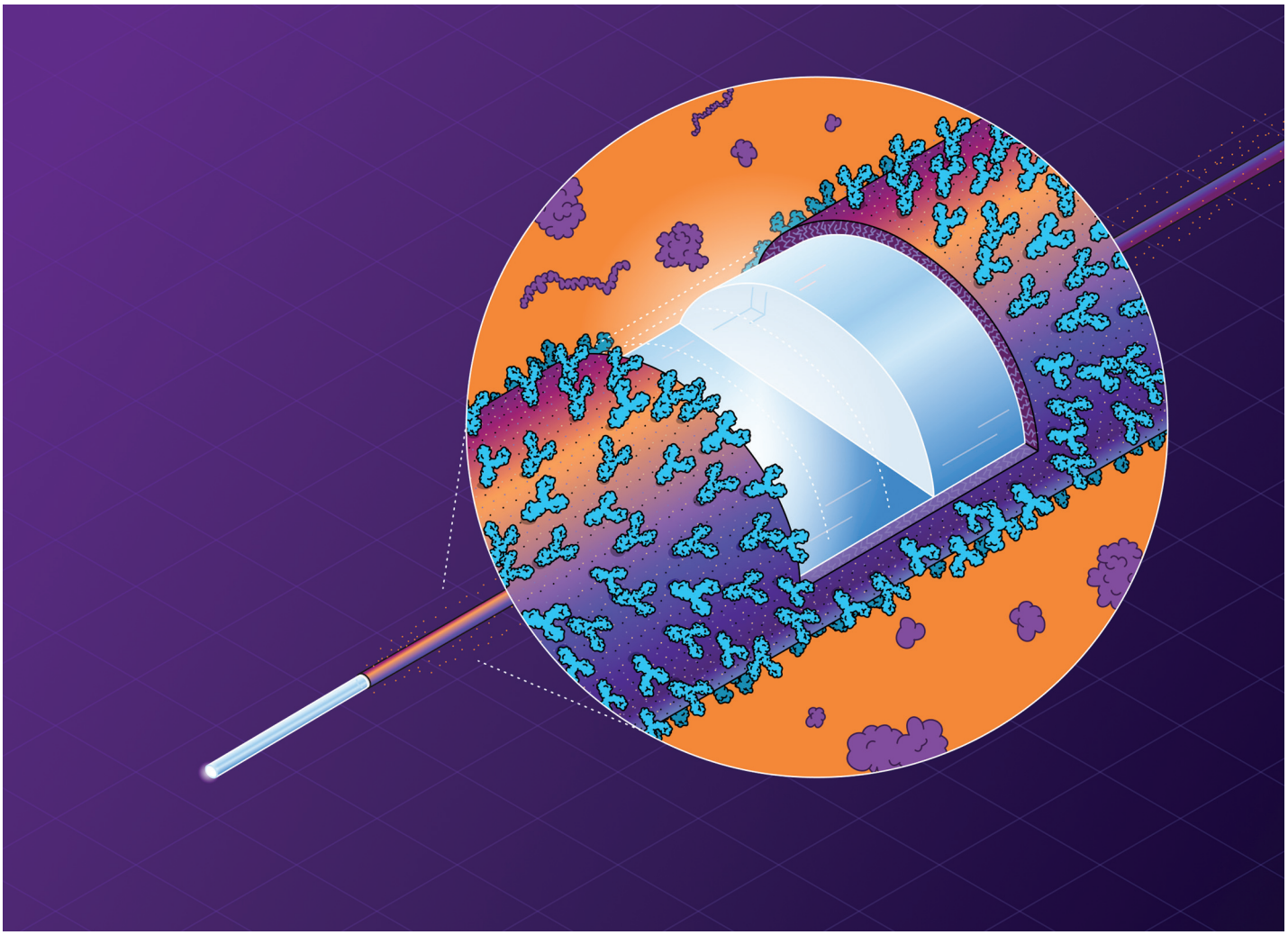

Showcasing research from Dr. Hana Vaisocherová-Lísalová's Laboratory of Functional Biointerfaces, FZU – Institute of Physics of the Czech Academy of Sciences, Prague, Czechia, and Dr. Francesco Chiavaioli from Chemical and Biochemical Optical Sensor Group, Institute of Applied Physics "Nello Carrara", National Research Council of Italy, Florence, Italy.

Optical fibre long-period grating sensors modified with antifouling bio-functional nano-brushes

Our study pioneers a post-modification strategy using terpolymer nano-brush grafted onto optical fibre long-period grating (LPG) sensors, achieving exceptional antifouling and biorecognition performance. We present direct synthesis of the nano-brush on LPG fibre sensors, ensuring their outstanding antifouling properties in complex media while enabling biorecognition element functionalization. The successful synthesis is confirmed *via* scanning electron microscopy, and the bioanalytical capabilities are demonstrated through fluorescence and label-free immunoassays. The terpolymer-coated LPG fibre sensors enable sensitive, real-time biomolecule detection in blood plasma, highlighting their potential for high-performance biosensing in healthcare and diagnostics.

As featured in:

See Francesco Chiavaioli, Hana Vaisocherová-Lísalová *et al.*, *Biomater. Sci.*, 2025, **13**, 1199.

ROYAL SOCIETY OF CHEMISTRY

rsc.li/biomaterials-science

Registered charity number: 207890

Biomaterials Science

ROYAL SOCIETY OF CHEMISTRY

PAPER

View Article Online
View Journal | View Issue

Cite this: *Biomater. Sci.*, 2025, **13**, 1199

Optical fibre long-period grating sensors modified with antifouling bio-functional nano-brushes†

Markéta Vrabcová, [a,b] Monika Spasovová, [a,b] Michala Forinová, [a,b] Ambra Giannetti, [c] Milan Houska, [a] N. Scott Lynn, Jr., [a] Francesco Baldini, [c] Jaromír Kopeček, [a] Francesco Chiavaioli *[c] and Hana Vaisocherová-Lísalová *[a]

Recent advances in optical sensing technologies underpin the development of high-performance, surface-sensitive analytical tools capable of reliable and precise detection of molecular targets in complex biological media in non-laboratory settings. Optical fibre sensors guide light to and from a region of interest, enabling sensitive measurements of localized environments. This positions optical fibre sensors as a highly promising technology for a wide range of biochemical and healthcare applications. However, their performance in real-world biological media is often limited by the absence of robust post-modification strategies that provide both high biorecognition and antifouling capabilities. In this study, we present the proof-of-concept antifouling and biorecognition performance of a polymer brush nano-coating synthesized at the sensing region of optical fibre long-period grating (LPG) sensors. Using a newly developed antifouling terpolymer brush (ATB) composed of carboxybetaine methacrylamide, sulfobetaine methacrylamide, and *N*-(2-hydroxypropyl)methacrylamide, we achieve state-of-the-art antifouling properties. The successful on-fibre ATB synthesis is confirmed through scanning electron microscopy (SEM), fluorescence microscopy, and label-free bio-detection experiments based on antibody-functionalized ATB-coated LPG optical fibres. Despite the challenges in handling optical fibres during polymerization, the resulting nano-coating retains its remarkable antifouling properties upon exposure to blood plasma and enables biorecognition element functionalization. These capabilities are demonstrated through the detection of IgG in buffer and diluted blood plasma using anti-IgG-functionalized ATB-coated sensing regions of LPG fibres in both label-based (fluorescence) and label-free real-time detection experiments. The results show the potential of ATB-coated LPG fibres for use in analytical biosensing applications.

Received 31st October 2024,
Accepted 10th December 2024

DOI: 10.1039/d4bm01447b

rsc.li/biomaterials-science

1. Introduction

The demand for accurate and rapid detection of molecular targets is becoming increasingly vital across various fields, including medical diagnostics, environmental monitoring, food control, forensics, and biotechnology. Continuous developments over the past 30 years have significantly advanced the analytical capabilities of optical, electrochemical, magnetic, and acoustic-based sensors.[1] Despite these tremendous advances, there remains a pressing need for enhanced analytical capabilities, particularly for portable devices intended for use in non-laboratory settings, operating in direct contact with complex biological media. This need became especially evident during the coronavirus pandemic in 2019, highlighting the urgency for developing high-performance, rapid, sensitive, reliable, and accurate novel analytical tools for the detection of molecules relevant to severe diseases. Addressing this challenge represents one of the significant priorities of our time.

Among all biosensing approaches, optical techniques based on resonant phenomena have been particularly successful in detecting biological entities at ultralow concentrations. These techniques operate through various sensing principles involving fluorescence, Raman spectroscopy, surface plasmon reso-

[a]*FZU – Institute of Physics, Czech Academy of Sciences, Na Slovance 2, Prague 182 00, Czechia. E-mail: lisalova@fzu.cz*
[b]*Institute of Physics, Faculty of Mathematics and Physics, Charles University, Ke Karlovu 3, Prague, 121 16, Czechia*
[c]*Institute of Applied Physics "Nello Carrara", National Research Council of Italy, Via Madonna del Piano 10, 50019 Sesto Fiorentino, Firenze, Italy. E-mail: f.chiavaioli@ifac.cnr.it*

†Electronic supplementary information (ESI) available: Manufacturing of long-period gratings; transmission spectra of LPG fibres before the deposition of terpolymer nano-brushes (Fig. S1); preparation of polymer nano-brushes; a photograph of reactors with the polymerization mixture (Fig. S2); a schematic of the terpolymer nano-brush architecture (Fig. S3); a step-by-step protocol for label-free experiments; Eudragit coating preparation; IR absorption spectra (Fig. S4); dry and wet thicknesses and swelling of a terpolymer nano-brush (Table S1); SPR results (Fig. S5); contact angle measurement results; EDS analysis results (Tables S2–S4). See DOI: https://doi.org/10.1039/d4bm01447b

nance (SPR), and other forms of optical resonance.[2] Optical fibre sensors leveraging these resonant phenomena are particularly promising for biochemical and healthcare applications.[3–5] By efficiently guiding light to and from a region of interest, they not only facilitate imaging and manipulation of local environments (*e.g.*, endoscopy, laser surgery, and imaging),[6,7] but also enable real-time monitoring of biological interactions in environments where other biosensing platforms may fall short.[8,9] Ultrasensitive optical fibre biosensors include those based on interferometry,[10] fibre gratings (both tilted fibre Bragg grating[11] and long-period grating (LPG)[12]), lossy mode resonance (LMR),[13] or those combined with SPR-active materials[9] or other nanomaterials.[14]

Despite the tremendous amount of work on fibre-based biosensors, there remain vast challenges that continue to limit their use in real-world applications outside the laboratory. Straightforward key challenges include enhancing the detection sensitivity through advanced nanofabrication or electronic improvements.[15] However, one of the most pressing issues is the nonspecific adsorption of biomolecules (fouling) onto the sensor surface when exposed to real-world detection media, such as blood plasma and serum. Though label-free fibre-based biosensors exhibit ultrasensitive capabilities, they often struggle to discriminate between target analytes and the fouled material. This challenge can complicate signal analysis and, more frequently, lead to performance deterioration. Research into surface-based biosensors has long addressed this issue, resulting in the development of various antifouling coatings that can be functionalized through the covalent attachment of biorecognition elements (BREs).[16,17]

One of the most promising antifouling materials for surface-sensitive biosensing is based on highly hydrophilic zwitterionic polymer coatings, which form brush-like structures.[16,18–21] The term "polymer brush" generally refers to ultrathin polymer coatings consisting of densely packed polymer chains, each anchored by one end to the sensing surface.[22,23] An ideal antifouling polymer brush (APB) should possess a high chain density to effectively shield the surrounding environment from interactions with the underlying support. Moreover, it should be highly hydratable, electroneutral, and biocompatible, while providing a high loading capacity for BREs and exhibiting sufficient thickness.[18] In biosensing applications, the thickness of APBs in dry state typically ranges from 15 to 40 nm, which is why these coatings are often referred to as nano-coatings or nano-brushes.[21,24,25] Zwitterionic polymer nano-brushes, particularly those synthesized from carboxybetaine (CB) compounds,[26] have been shown to meet all these criteria, establishing them as one of the cutting-edge materials for modern antifouling biosensor coatings.[16,17] Furthermore, CB-based polymer brushes have demonstrated remarkable long-term stability, particularly with respect to the impact of storage conditions on their antifouling performance and biorecognition loading capacity.[27,28] This stability underscores their ability to retain essential functional properties over extended storage periods, making them highly reliable for biosensing applications.

Despite their proven success in planar biosensing devices, the integration of APBs within optical fibre sensors remains significantly underexplored.[29] This gap likely stems from inherent challenges posed by the physical structure of optical fibre, often tens of centimetres in length, and the methods required for synthesizing and characterizing polymer brushes. The most effective highly-dense brushes are typically synthesized *via* surface-initiated atom transfer radical polymerization (ATRP), a *grafting from* process that requires controlled inert conditions using vacuum gas manifolds.[30] In this procedure, an initiator-bearing sensor is fully immersed in a reaction vessel containing monomer and catalyst solutions. For CB-based brushes, the high cost of monomers necessitates minimizing dead volume in the reaction vessel to ensure efficiency, a straightforward task for planar surfaces but much more difficult when dealing with fragile, high-aspect-ratio fibres, which can range from 10 to 100 cm in length and have diameters of only hundreds of microns. To our current knowledge, there is only one study on the use of an APB-coated optical fibre;[29] however, that study utilized coatings restricted to the fibre tip: a vastly different situation with respect to an LPG-based sensor, whose sensitive region (a few cm long) is located near the centre of a longer piece of fibre. In addition to challenges in polymerization, there are challenges in the characterization of coated fibres; typical methods based on infrared/Raman spectroscopy, atomic force microscopy, contact angle analysis, and ellipsometry are either incompatible with the small diameter of a fibre or require extensive modifications or procedures not available to most laboratories.

In this proof-of-concept study, we synthesize and characterize an antifouling terpolymer brush (hereafter ATB) polymerized from the sensitive surface region of an optical fibre LPG sensor. This innovative nano-coating is based on a terpolymer of carboxybetaine methacrylamide (CBMAA), sulfobetaine methacrylamide (SBMAA), and *N*-(2-hydroxypropyl)methacrylamide (HPMAA) and has previously shown excellent antifouling efficiency in a variety of complex media.[16,31] We show that despite the challenges related to the handling of optical fibres during the polymerization process, the resulting ATB-coated LPG fibre exhibits antifouling characteristics when exposed to blood plasma and can be effectively functionalized with BREs for affinity-based detection. The use of this optical fibre LPG sensor is demonstrated by the detection of a model biomarker (anti-IgG*) in both buffer and diluted blood plasma, as accomplished *via* fluorescence-labelled and label-free real-time experiments. The study shows the potential use of ATP-coated fibre sensors for analytical biosensing applications.

2. Materials and methods

2.1 Chemical reagents and materials

A photosensitive boron–germanium co-doped fibre (Fibercore PS1250/1500) was purchased from Fibercore, Humanetics, United Kingdom. The thiol-based initiator (11-mercaptoundecyl-2-bromo-2-methylpropanoate) and the bromo-silanes

((MeO)$_3$-Si-(CH$_2$)$_{11}$-Br) were from ProChimia Surfaces, Poland. The monomers carboxybetaine methacrylamide (CBMAA), sulfobetaine methacrylamide (SBMAA), and *N*-(2-hydroxypropyl) methacrylamide (HPMAA) were purchased from Specific Polymers, France. Other chemicals for polymerization, 1,4,8,11-tetramethyl-1,4,8,11-tetraazacyclotetradecane (Me$_4$cyclam, 98%), copper(I) chloride (CuCl, ≥99.995%), copper(II) chloride (CuCl$_2$, 99.999%), bovine serum albumin (BSA), methanol (≥99.9%), ethanol (99.9%), acetone (p.a.) and isopropanol (p.a.), were used as purchased from Merck, Czechia. Heptane (anhydrous, max. 0.003% water) was from VWR International, Czechia, and was opened just before use. Eudragit L 100, a 1 : 1 copolymer of methacrylic acid and methyl methacrylate, was purchased from Evonik Degussa GmbH (Dusseldorf, Germany). Water-based solutions were prepared from ultrapure water (18.0 MΩ cm, Milli-Q® system, Merck, Czechia). Chemicals for the preparation of phosphate-buffered saline (PBS, 0.01 M phosphate buffer, 0.137 M sodium chloride, 0.0027 M potassium chloride, pH 7.4 at 25 °C) and HEPES (4-(2-hydroxyethyl)-1-piperazineethane-sulfonic acid, 5 mM, pH 7 at 25 °C) were purchased from Merck, Czechia. Activation agents, *N*-hydroxysuccinimide (NHS), and *N*-ethyl-*N*′-(3-dimethyl-aminopropyl)carbodiimide (EDC), were obtained from Cytiva, Sweden, and were dissolved in ultrapure water before use (0.1 M and 0.5 M, respectively). 2-(2-Aminoethoxy)acetic acid (AEAA) was purchased from AlfaAesar, Germany, and was dissolved in ultrapure water before use (1 M, pH 7). Human blood plasma (pooled, mixed gender, pH 7.9) in sodium citrate was purchased from VWR International, Czechia, and was stored at −20 °C before use. Mouse IgG and labelled goat anti-mouse IgG* (* indicates the fluorescent label AlexaFluor 647, λ_{ex} = 650 nm, λ_{em} = 665 nm) antibodies for fluorescence experiments were purchased from ThermoFisher Scientific, Milan, Italy. Anti-*E. coli* O157:H7 (anti-*E. coli*) antibodies, used as reference antibodies for SPR measurements, were purchased from KPL Inc., USA.

2.2 Optical fibre sensor setup

Five different standard LPG fibres were manufactured for this study; their transmission spectra are shown in Fig. S1.† Despite the different values of the LPG resonance wavelength (λ_{LPG}; *i.e.*, the wavelength minimum of the resonance band), we considered and used the same cladding mode (*i.e.*, 7th cladding mode) for all experiments, and hence we did not face any issue of different sensitivity between fibres, since in this mode these LPG fibres should possess similar refractive index sensitivity on the order of tens of nm per RIU. Further details on the manufacturing methods and optical characterization can be found in the ESI.†

The experimental setup employed for real-time analysis (including characterization) is depicted in Fig. 1. Light was coupled into the optical fibre using a multi-LED light source (SLD1310/1430/1550/1690, Fibrelabs, Inc., Saitama, Japan), whereas the output from the fibre was connected to an optical spectrum analyser (OSA; MS9030A/9701C, Anritsu, Kanagawa, Japan), which collected the transmission spectrum and enabled the measurement of λ_{LPG} in the range of 1250–1700 nm. Each ATB-coated LPG fibre was placed inside a

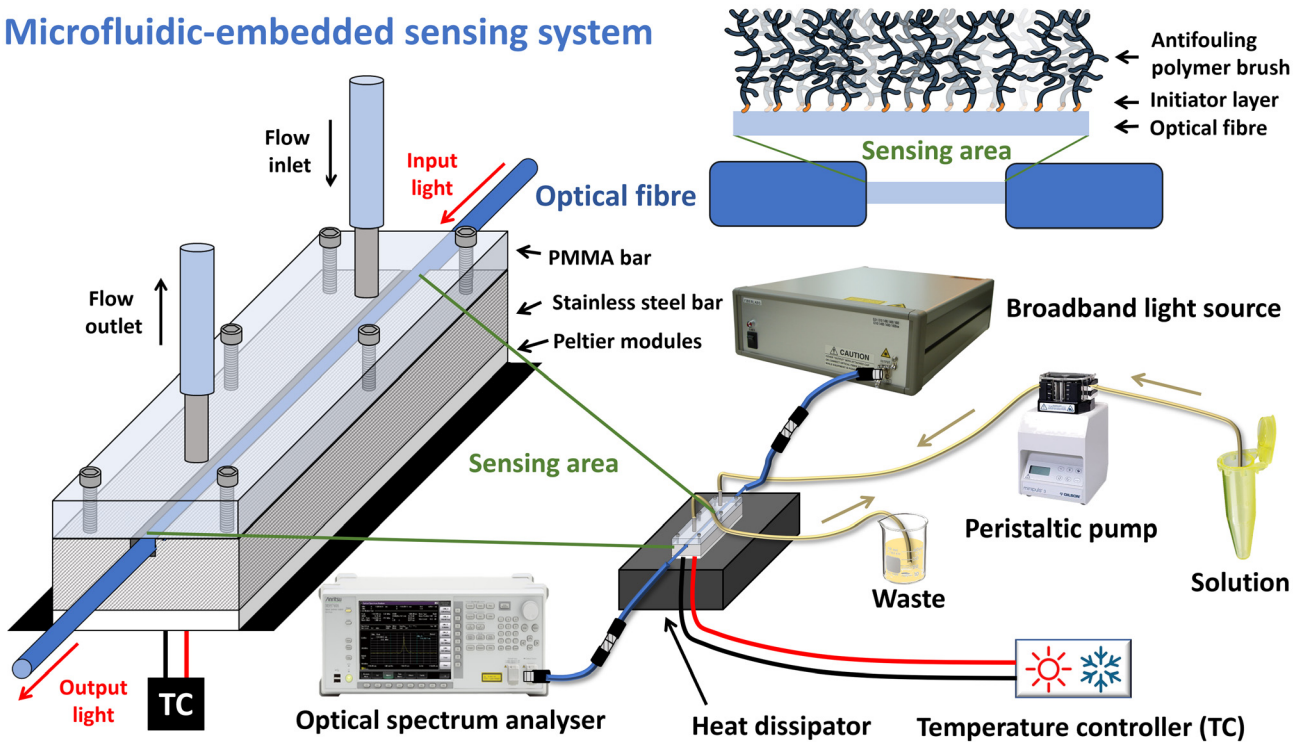

Fig. 1 General schematic of the fibre-optic sensing system used herein.

custom-made microfluidic system that allowed for small volume injections (tens of μL) while maintaining a stable temperature (±0.05 °C) *via* the use of two Peltier cells (15 cm width, 30 cm length) and a thermistor inserted into a lateral hole of a stainless steel bar to provide feedback to a control unit (TEC controller, LDC-3722B, ILX Lightwave, MT, USA); further details can be found in the literature.[32] The flow channel was connected to a peristaltic pump *via* medical-grade PVC tubing (0.76 mm inner diameter) used to inject the solutions into the microfluidic system. The temperature of the flow channel was measured using a thermocouple connected to a thermometric measuring unit (Lutron TM-917, Lutron Instruments, Taiwan) and placed inside the PMMA bar as close as possible to the flow channel.

2.3 Preparation of terpolymer nano-brushes

The random terpolymer nano-brush was grafted from the sensitive regions of LPG fibres using surface-initiated ATRP following a previously published procedure.[31] Prior to polymerization, fibres having coiled ends were cleaned, silanized (to form an initiator layer), rinsed with water, and dried before being inserted into two polymerization reactors (one for each fibre; see Fig. S2A and B†) that were subsequently filled with polymerization solution. In parallel, ATBs were also prepared onto gold-coated glass slides within the same polymerization reactors, which were used as a control. The polymerization was conducted for 2 h, after which all samples were washed with ultrapure water and stored in PBS at 6 °C until further use. More details on the polymerization procedure and the molecular structure of the terpolymer nano-brush (Fig. S3†) are given in the ESI.†

2.4 Immunoassay protocols for fluorescence and label-free experiments

For fluorescence-based experiments, one ATB-coated LPG fibre was cut in two pieces, with one part used for an immunoassay experiment in PBS and the second part for an immunoassay experiment in 10% human blood plasma diluted in PBS. All fluorescence experiments were conducted *ex situ* by fibre immersion into vials holding respective solutions. First, both fibre pieces were immersed in ultrapure water and PBS (subsequently for 30 min) to rehydrate the ATB coatings. The carboxyl groups on the terpolymer were then activated *via* immersion in an EDC/NHS solution for 20 min, washed with ultrapure water, and immersed for 1 h in mouse IgG solution (0.5 mg mL^{-1} in borate buffer 10 mM, pH 8) to functionalize the ATB with IgG antibodies. After a 5 min wash with ultrapure water, the fibres were immersed in AEAA (1 M, pH 7) for 25 min to deactivate the non-reacted carboxy-functional groups. Finally, the fibres were washed with ultrapure water. After this functionalization procedure, one piece of fibre was immersed in PBS and the second piece was immersed in human blood plasma (10% diluted in PBS) for 15 min, the results of both thus simulating an anti-mouse IgG* concentration of 0 mg L^{-1}. LPG fibres were then exposed to increasing concentrations of anti-mouse IgG* in respective solutions (from 0.1 mg L^{-1} to 100 mg L^{-1}), with a 5 min wash in PBS between each step. Fluorescence measurements of the LPG fibres were performed using a commercial fluorescence microscope based on a Zeiss Axio Observer Fluorescence Microscopy System (Zeiss, Jena, Germany) with 5× and 0.12 numerical aperture objective lens, Colibri source system (LED at 625 nm), and integration time 1 s. The fluorescence intensity, represented by the brightness of the measured image pixels, was calculated using the microscope software, recording the fluorescence signal after every interaction with the anti-mouse/IgG* AlexaFluor 647 including the washing step.

The label-free experiments were carried out using the experimental setup shown in Fig. 1. A step-by-step protocol for the detection of anti-mouse IgG in diluted blood plasma (10% in PBS) is detailed in the ESI.† In these experiments, the minimum of the resonance band at longer wavelengths (corresponding to 7^{th} cladding mode) in the transmission spectrum of the LPG fibre was monitored in real time, with a data acquisition step of 10 s. The temperature of the microfluidic system was set to 22 °C. The peristaltic pump and the microfluidic system enabled adjustment of the flow rate from 10 μL min^{-1} to 250 μL min^{-1}. A higher flow rate of 150 μL min^{-1} was used during rinsing steps in running buffer, whereas a lower flow rate of 35 μL min^{-1} was used during the injection of biological solutions. After each rinsing step, the flow was stopped and approx. 30 experimental points were collected within 5 min. The difference of the average maximum-absorption wavelength during this stage with respect to the average maximum-absorption wavelength before the IgG binding is representative of the surface density of captured anti-mouse IgG on the fibre surface.

2.5 Characterization of the terpolymer nano-brush

2.5.1. Infrared reflection–absorption spectroscopy (IRRAS). The presence of the ATB on control substrates (gold-coated BK7 glass slides) was confirmed by infrared reflection–absorption spectroscopy (IRRAS) using the Thermo Scientific™ Nicolet™ iS50 FTIR spectrometer equipped with Smart SAGA™ Accessory. The spectra were collected with 200 scans at 4 cm^{-1} resolution and 80° reflection angle from approximately 1 cm^2 surface area. Before the infrared measurements, samples were rinsed with ultrapure water and dried with a flow of nitrogen. IRRAS spectra are provided in the ESI (Fig. S4†).

2.5.2. Scanning electron microscopy (SEM) and energy-dispersive X-ray spectroscopy (EDS). Scanning electron microscopy (SEM) and energy-dispersive X-ray spectroscopy (EDS) of coated optical fibres were performed on a Tescan FERA 3 microscope and an EDAX Octane Super 60 mm^2 analyser. Imaging using these methods was performed in order to confirm the deposition of ATB onto the fibre and to characterize the nano-brushes in terms of homogeneity and elemental analysis.

2.5.3. Spectroscopic ellipsometry (SE). The thickness of ATB and its change in water due to the absorption of water molecules between the polymer chains, *i.e.* swelling, were characterized on a control gold substrate using a spectroscopic ellips-

ometer (VASE, J. A. Woollam, Lincoln, USA) in the spectral range of 300–1000 nm with steps of 10 nm and a 70° angle of incidence. Data analysis was performed with WVASE32 software; experimental data were fitted with a single Gaussian oscillator model as described in our previous work.[33] Results from SE measurements are shown in the ESI (Table S1†).

2.5.4. Surface plasmon resonance (SPR). SPR experiments on ATB-coated control substrates were performed on a 4-channel multiparametric SPR sensor (BioNavis Ltd, Finland) using a light-emitting diode source of 785 nm. Surface mass densities were determined from angular units (corresponding to the shift in the SPR resonance angle) using the following equation: 0.001° = 0.85 ng cm^{-2}. More details and results of the SPR experiments can be found in the ESI (Fig. S5†).

2.5.5. Contact angle measurement. The wettability of the coating was determined on ATB-coated control substrates by contact angle measurements in ultrapure water using Drop Shape Analyzer 100 (Krüss, Germany). Details of the analysis, including results, are provided in the ESI.†

3. Results and discussion

3.1 Verification and characterization of ATB coatings on LPG fibres

3.1.1 SEM and EDS analyses. The presence of ATB on LPG fibres was confirmed through SEM and EDS. Fig. 2 provides a comparison of SEM images for both a bare optical fibre and an ATB-coated LPG fibre, revealing the presence of a polymer coating layer on the latter. Furthermore, the ATB-coated LPG fibre displays two distinct regions: (i) areas where the ATB coating appears sparse (area 1 in Fig. 2b) and (ii) areas where the ATB layer is thicker, but not completely homogeneous (area 2 in Fig. 2b). To further support these observations and confirm successful ATB deposition, a high-magnification SEM image was captured in a region with more effective nano-brush deposition, and five distinct spots were analysed using EDS (Fig. 2c).

It is important to note that while EDS in semi-quantitative mode has limitations in the analysis of organic materials, primarily due to its reduced sensitivity to light elements, it still provides qualitative insights into the presence of the nano-brush. The nano-brush used in this study consist mainly of carbon and nitrogen atoms, while the optical fibres are composed mainly of silicon oxide. The atomic percentages of elements identified at different spots are provided in the ESI (Tables S2–S4†), with a calculation of the ratio between carbon and silicon atoms (C/Si) serving as an indicator of the brush-to-glass ratio. The presence of silver and copper originates from the adhesive used to secure the fibre sample in the SEM holder, and the content of aluminium can be attributed to the material of the SEM sample holder (a standard SEM stub). Regions where the nano-brush layer was thinner or damaged (appearing smoother in Fig. 2) showed lower carbon and higher silicon, oxygen, and aluminium content, whereas more homogeneously coated areas exhibited the opposite trend. Notably, regions with a carbon content exceeding 50% and a C/Si ratio greater than 9% indicate areas where polymerization occurred reliably and effectively.

Although the spots in Fig. 2c, taken from seemingly well-covered regions of the fibre, detail a similar but not identical C/Si ratio, slight inhomogeneities in the coating are apparent. These ATB non-uniformities likely stem from both the complex cleaning and multi-step preparation processes required for handling the fibres, as well as from the incompatibility of placing a long, coiled fibre into a glass vessel designed for smaller substrates. To address these issues, future work will focus on simplifying the process to minimize inhomogeneities and improve the quality of the ATB coating by developing an in-flow polymerization system within glass tubes better suited for long fibres (*e.g.*, long capillary tubes). Despite the coating inhomogeneity, the overall findings confirm that polymerization successfully occurred on most of the LPG fibre sensing surface, demonstrating the feasibility of the developed polymerization method.

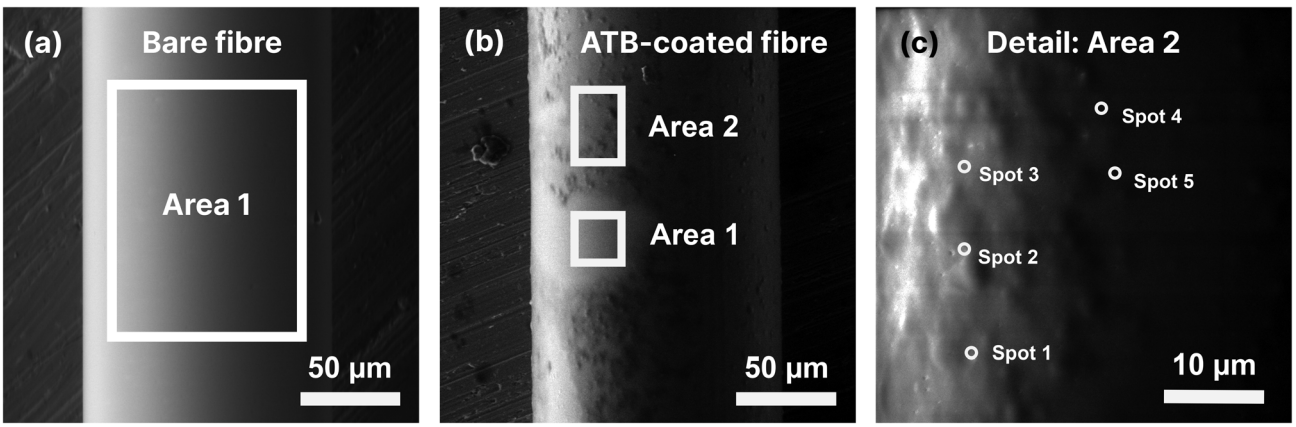

Fig. 2 (a) SEM image of a bare optical fibre; (b) SEM image of an ATB-coated LPG fibre with selected areas for EDS analysis: area 1 shows very smooth surface and pertains to an area of the fibre where the polymerization did not run properly, whereas area 2 confirms the presence of terpolymer nano-brush; (c) enlarged SEM image of area 2 of the ATB-coated LPG fibre with 5 selected spots for EDS analysis.

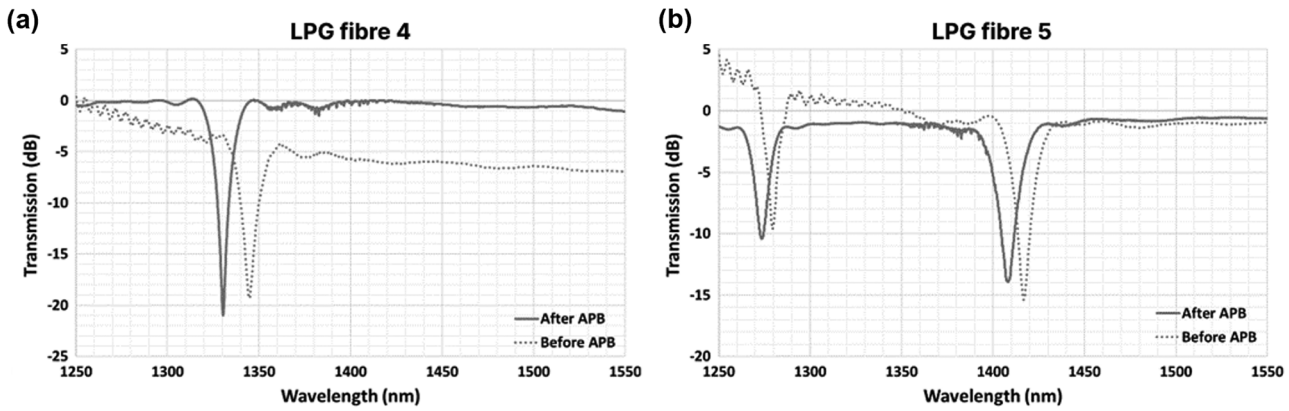

Fig. 3 Transmission spectra of optical fibres (measured in air): LPG fibre 4 (a) and LPG fibre 5 (b) before (dotted grey curve) and after (grey curve) the deposition of ATB coatings.

3.1.2 Characterization of ATB-coated control planar substrates. Characterizing thin coatings on long coiled-like LPG fibres by standard characterization techniques presents significant challenges (as discussed earlier). To facilitate more accessible characterization, we polymerized ATB on planar gold-coated glass slides, which are more amenable to various techniques. The planar control samples are compatible with standard nano-brush characterization methods, and as they had similar Br-based initiator layers to the fibre samples, they represent a convenient method to confirm brush structure and thickness. The IRRAS spectra (Fig. S4†) confirm the presence of contaminant-free ATB on the reference substrates. Contact angle measurements indicate strong hydrophilic behaviour (17.8° ± 2.4°), while SE data (Table S1†) show a brush thickness suitable for obtaining antifouling and BRE loading capacities (dry film: (25.7 ± 0.5) nm, wet film: (79.5 ± 0.8) nm, swelling ratio: 3.09 ± 0.07). In addition, the SPR data taken from the control sample show that the ATB coatings have a high antibody loading capacity (182 ng cm^{-2}) and maintain excellent resistance to fouling from undiluted blood plasma (5.9 ng cm^{-2}). Overall, these results align well with previously published data on ATBs,[24,31,34] confirming the formation of a high-quality, functionalizable ATB layer on the reference substrates.

3.1.3 Characterization *via* LPG resonance. Finally, we characterized the ATB coatings on LPG fibres *via* changes in the resonant response of fibres after polymerization. For this, we note that the change of resonant frequency upon coating of LPG sensors with a nano-brush is observed during modal transition,[35] which is a process of deposition of an additional nanoscale layer with the refractive index (RI) higher than that of the fibre material, in order to enhance the performance of LPGs. The degree of enhancement in this case depends on the optical properties of the coating, especially its thickness and RI, where such coatings lead to spectral shifts in the LPG resonance band towards shorter wavelengths. This principle can also be used to experimentally confirm the deposition of ATB onto a fibre. Hence, to verify the ATB deposition, we recorded the transmission spectra of LPG fibres before polymerization (in air) and after polymerization (in air and water).

Fig. 3 presents the before/after results for two LPG fibres, with detailed results summarized in Table 1. As expected, both fibres showed a distinct spectral shift of λ_{LPG} towards shorter wavelengths; in this situation a larger shift corresponds to a thicker ATB. We observed small changes in the resonant shift between the two fibres (9.4 nm and 10.4 nm, 11% difference). Measurements in water further led to a smaller λ_{LPG} shift for each coating, with a similar %-difference between samples (3.0 nm and 3.4 nm, 13% difference), which under the same assumptions would indicate further increases in the brush thickness due to swelling effects.

It is important to note that the discrepancies in wavelength shifts between fibres could result from differences in both the coatings' physical (thickness) or optical (RI) properties, or alternatively, variations in the ATB homogeneity. Regardless, these data indicate that simple analysis of the LPG spectra can be used as a characterization tool for such nano-brushes. A full examination of changes to the optical or physical properties of a polymer nano-brush can be carried out using dedicated software tools (*i.e.*, COMSOL, FIMMWAVE or OPTIWAVE) – which is well beyond the scope of this article – and will be the focus of future research.

3.2 Fluorescence immunoassay

Further characterization of the ATB-coated LPG fibres was performed using fluorescence microscopy on two separate portions of the fibres. This assay not only confirmed successful

Table 1 Comparative results on the ATB deposition on two LPG-embedded fibre samples

Sample	Bare optical fibre (nm)	Optical fibre with ATB (nm)			
	λ_{LPG_air}	λ_{LPG_air}	$\lambda_{LPG\_H_2O}$	$\lambda_{LPG\_air\text{-}H_2O}$	λ_{LPG_air} (nm)
LPG fibre 4	1344.6	1334.2	1330.8	3.4	10.4
LPG fibre 5	1417.6	1408.2	1405.2	3.0	9.4

polymerization but also evaluated the nano-brush potential for affinity-based detection. This fluorescence immunoassay consisted of functionalizing both fibre portions with IgG antibodies and measuring the response to fluorescently labelled anti-mouse IgG* in a step-by-step fashion (a static immersion in anti-mouse IgG* solution, proceeding from low to high concentrations). Fig. 4 shows a direct comparison of the fluorescence results obtained with anti-mouse IgG* spiked in PBS and anti-mouse IgG* spiked in 10% plasma (diluted in PBS). Both the qualitative and quantitative nature of these data provide information regarding the ATB coatings. Firstly, the data from both PBS and diluted plasma indicate consistent increases in fluorescence signal with increases in anti-mouse IgG* concentration (with both following the same power law trends), which suggests that the capture of anti-mouse IgG* occurs *via* a selective mechanism. In addition, data from the diluted plasma experiments are slightly lower than those taken from PBS experiments (*i.e.*, similar ratio across all concentrations), a trend that is exhibited by other affinity-based assays carried out on antifouling coatings.[26] The nature of this signal drop is due to a lowered probability for the analyte to reach the sensing surface due to a more intense electric charge effect over the biomolecules and/or to a denser matrix. Finally, the comparable values in the blank samples (127 a.u. and 121 a.u. for PBS and diluted plasma, respectively) indicate the extraordinary antifouling performance of the ATB.

3.3 Label-free LPG immunoassay

Finally, we carried out a label-free version of the immunoassay described in section 3.2 in diluted plasma (albeit in the arrangement shown in Fig. 1) by tracking the resonant LPG feature over time. Fig. 5a illustrates the post-modification of the ATB-coated LPG fibre, specifically the activation of carboxyl groups of ATB *via* EDC/NHS chemistry, the immobilization of IgG antibodies, and the subsequent deactivation of IgG-functionalized ATB by a deactivating agent (AEAA).

Fig. 5b details a real-time detection experiment performed on an IgG-functionalized ATB-coated LPG fibre. To evaluate its antifouling properties after IgG functionalization, the fibre was first exposed to diluted plasma. Subsequently, the sensor was exposed to three solutions of diluted plasma with 10× increases in anti-IgG concentration (0.01, 0.1, 1 mg L^{-1}). This assay was conducted in a manner that measurements were taken during periods of stopped flow (after a PBS washing step) to lower the noise and maintain a constant temperature. Artifacts in the sensing signal (in the form of spikes) are attributed to short increases in flow to remove unwanted bubbles in the microfluidic channel. The dotted lines in Fig. 5 represent the temperature evolution throughout the experiment, revealing a total variation of less than 0.2 °C, which minimizes the temperature cross-sensitivity effect on the λ_{LPG} shift caused by the RI changes.

The dose–response curve for these data is shown in Fig. 5d. Experimental points for different concentrations of anti-IgG spiked in diluted plasma (blue squares) and in PBS (orange triangle) are presented with their relative standard deviation, whereas the grey curve represents the fitting curve based on a widely used logistic equation (non-linear function) to describe antibody–antigen binding.[36] The calculated limit of detection was 32 μg L^{-1} which, though based on limited data, represents a significant improvement over previous results using similar assays and LPG fibre sensors.[37]

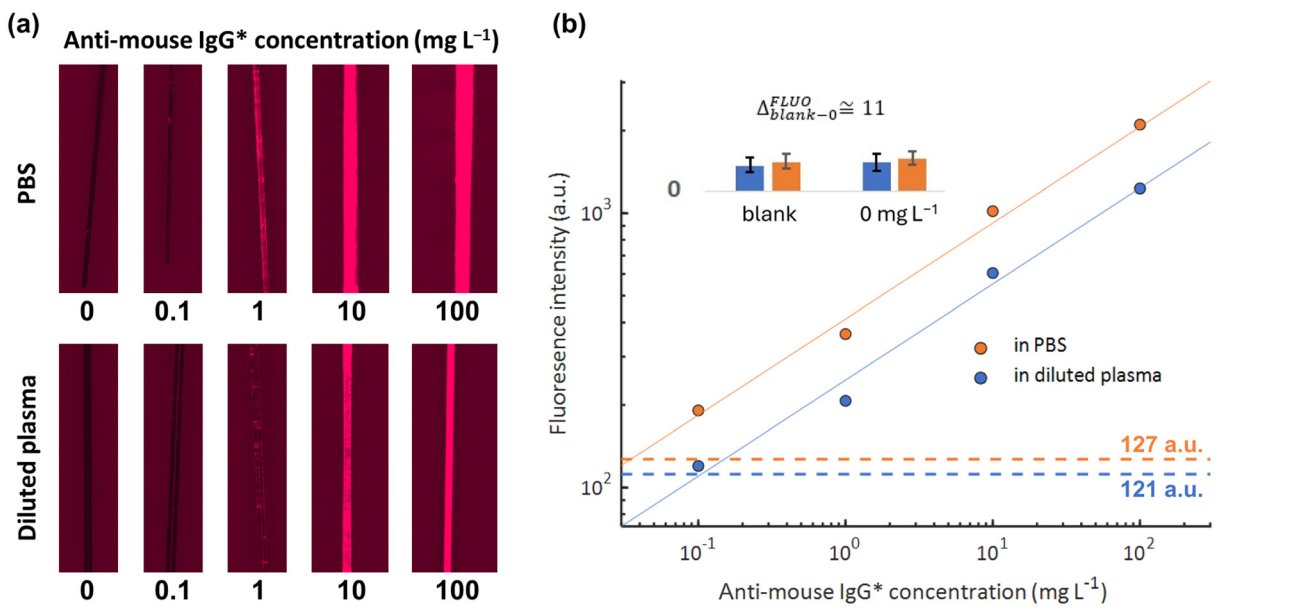

Fig. 4 (a) Fluorescence microscopy images of LPG fibres exposed to increasing concentrations of anti-mouse IgG* in PBS (top row) and in diluted plasma (bottom row); (b) dependence of fluorescence intensity on anti-mouse IgG* concentration measured on ATB-coated LPG fibres in PBS (orange) and in 10% human blood plasma diluted in PBS (blue).

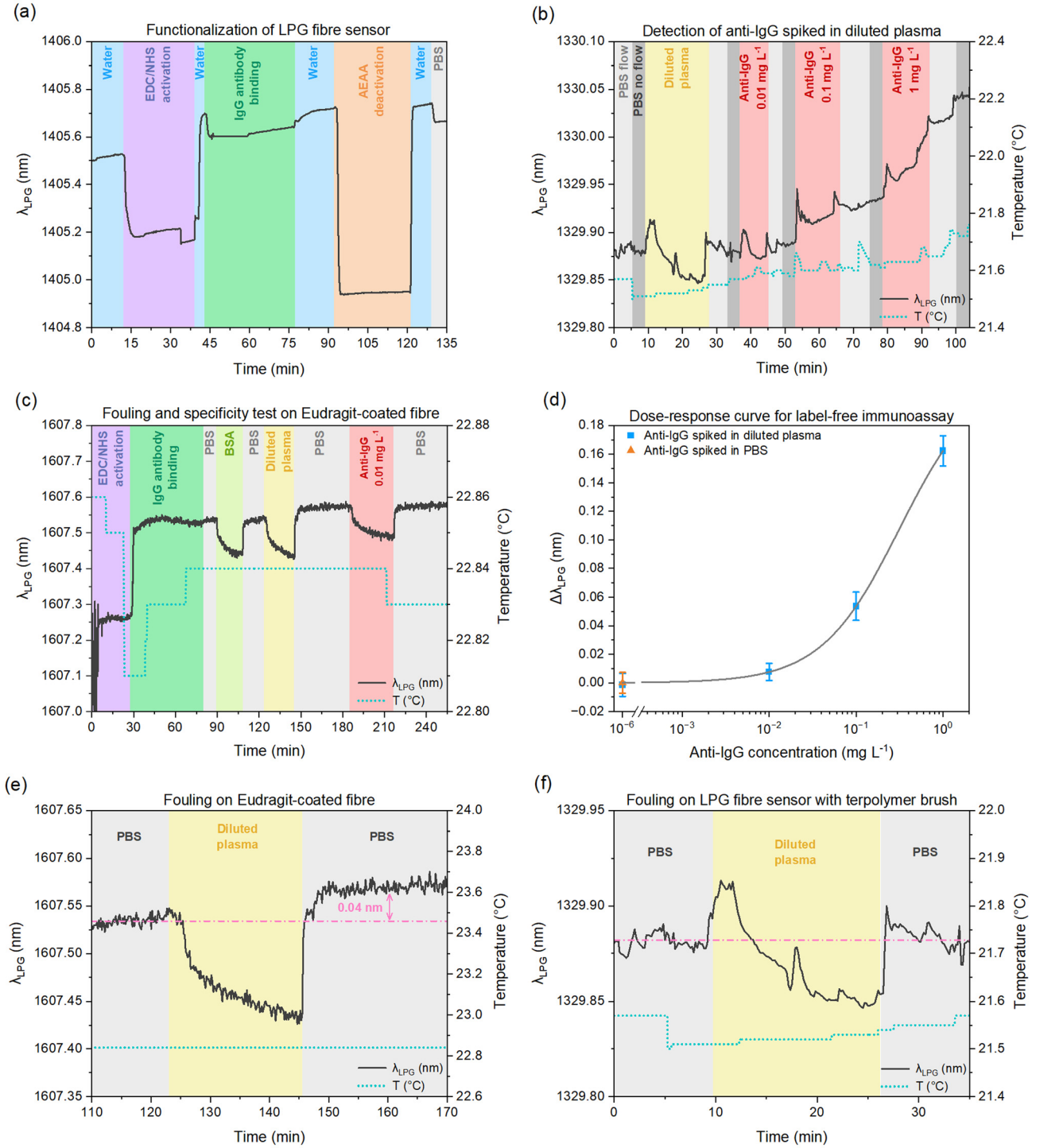

Fig. 5 Sensorgrams of the label-free immunoassay: (a) illustrative data on functionalization of the ATB on the LPG fibre sensor with IgG antibodies; (b) detection of anti-IgG spiked in diluted plasma; (c) fouling and specificity test on an Eudragit-coated fibre passivated using BSA; (d) dose–response curve for anti-IgG spiked in diluted plasma (blue squares) and in PBS (orange triangle); details of the plasma fouling test performed on an Eudragit-coated optical fibre (e) and an ATB-coated LPG fibre (f).

To assess the antifouling performance of our ATB on LPG fibre, we compared it with another fibre coating using Eudragit L 100. Eudragit L 100 is a 1 : 1 copolymer of methacrylic acid and methyl methacrylate and it has already been used for a model assay on fibre sensors.[32,38] The LPG fibre was coated by immersion in an Eudragit L 100 solution to form a dry layer 60 nm thick, functionalized with IgG antibodies, and then passivated against nonspecific inter-

actions with BSA. The whole procedure is described in the ESI.†

The differences in antifouling capability between ATB-coated and Eudragit-coated LPG fibres are demonstrated in Fig. 5e and f. After the injection of diluted blood plasma, the resonant signal for the Eudragit-coated fibre showed a shift in λ_{LPG} of 0.04 ± 0.008 nm (Fig. 5e), while only 0.001 ± 0.003 nm (Fig. 5f) for the ATB-coated fibre. The significance of this difference in fouling is further amplified when put into the context of the selective λ_{LPG} shift due to anti-IgG binding seen in Fig. 5d; the signal from fouling of 0.04 nm would cause a false positive result of ~0.1 mg mL^{-1}.

4. Conclusions

In this study, we pioneered the optical LPG fibre post-modification strategy based on an antifouling terpolymer nanobrush. Specifically, we investigated the performance of an ATB composed of *N*-(2-hydroxypropyl)methacrylamide, carboxybetaine methacrylamide, and sulfobetaine methacrylamide, which was grafted onto fragile, long, coiled optical LPG fibres with the sensing region located in the central area of the fibre. Post-polymerization, the ATB-coated fibres were successfully functionalized with IgG antibodies, resulting in an excellent combination of antifouling and biorecognition performance, even in complex biological media represented herein by human blood plasma. The selectivity and sensitivity of the LPG fibres were demonstrated using both fluorescence-based and label-free immunoassays in blood plasma. The results pave a new avenue for the transition of ultrasensitive fibre-optic technologies towards real-world bioanalytical and biomedical applications.

Author contributions

M. V.: writing – original draft, investigation, methodology, data curation, formal analysis, visualization, and funding acquisition. M. S.: investigation, data curation, and formal analysis. M. F.: investigation, data curation, formal analysis, and funding acquisition. A. G.: investigation, data curation, and writing – review & editing. M. H.: investigation, data curation, and writing – review & editing. N. S. L. and F. B.: writing – review & editing. J. K.: investigation, data curation, formal analysis, and funding acquisition. F. C.: investigation, data curation, formal analysis, methodology, writing – review & editing, supervision, and funding acquisition. H. V.-L.: conceptualization, writing – review & editing, supervision, and funding acquisition.

Data availability

Data for this article are available at Zenodo repository (**https://doi.org/10.5281/zenodo.14034212**).

Conflicts of interest

There are no conflicts of interest to declare.

Acknowledgements

This work was supported by the Bilateral Agreement between the National Research Council of Italy (CNR) and the Czech Academy of Sciences (CAS) under the mobility project "High-performance nanolayer-coated fibre-based biosensing platforms with antifouling brushes for detection of post-acute COVID-19 syndrome biomarkers in blood plasma" (CNR-22-28), the Czech Science Foundation (24-10671S), and the Operational Programme Johannes Amos Comenius financed by the European Structural and Investment Funds and the Czech Ministry of Education, Youth and Sports (project SENDISO CZ.02.01.01/00/22_008/0004596). M. V. and M. F. were supported by the grant from Charles University (SVV-2023-260716). We acknowledge the CzechNanoLab Research Infrastructure supported by MEYS CR (LM2023051) for SEM usage.

References

1 C. I. L. Justino, A. C. Duarte and T. A. P. Rocha-Santos, *TrAC, Trends Anal. Chem.*, 2016, **85**, 36–60.
2 A. K. Singh, S. Mittal, M. Das, A. Saharia and M. Tiwari, *Alexandria Eng. J.*, 2023, **67**, 673–691.
3 Y. Zhang, J. Zheng, F. Jin, J. Xiao, N. Lan, Z. Xu, X. Yue, Z. Li, C. Li, D. Cao, Y. Wang, W. Zhong, Y. Ran and B. O. Guan, *Light: Sci. Appl.*, 2024, **13**, 228.
4 L. Zu, X. Wang, P. Liu, J. Xie, X. Zhang, W. Liu, Z. Li, S. Zhang, K. Li, A. Giannetti, W. Bi, F. Chiavaioli, L. Shi and T. Guo, *Adv. Sci.*, 2024, **11**, 2308783.
5 S. Cao, R. Chen, Q. Yang, X. He, F. Chiavaioli, Y. Ran and B.-O. Guan, *Biosens. Bioelectron.*, 2024, **249**, 116014.
6 M. Rezapour Sarabi, N. Jiang, E. Ozturk, A. K. Yetisen and S. Tasoglu, *Lab Chip*, 2021, **21**, 627–640.
7 Y. Ran, Z. Xu, M. Chen, W. Wang, Y. Wu, J. Cai, J. Long, Z.-S. Chen, D. Zhang and B.-O. Guan, *Adv. Sci.*, 2022, **9**, 2200456.
8 C. Caucheteur, T. Guo, F. Liu, B.-O. Guan and J. Albert, *Nat. Commun.*, 2016, **7**, 13371.
9 L. Liu, X. Zhang, Q. Zhu, K. Li, Y. Lu, X. Zhou and T. Guo, *Light: Sci. Appl.*, 2021, **10**, 181.
10 T. Zhu, K. Chah, F. Chiavaioli, J. Villatoro and C. Caucheteur, *Opt. Laser Technol.*, 2024, **168**, 109878.
11 J. Albert, L.-Y. Shao and C. Caucheteur, *Laser Photonics Rev.*, 2013, **7**, 83–108.
12 F. Esposito, A. Srivastava, L. Sansone, M. Giordano, S. Campopiano and A. Iadicicco, *IEEE Sens. J.*, 2021, **21**, 12692–12705.
13 F. Chiavaioli and D. Janner, *J. Lightwave Technol.*, 2021, **39**, 3855–3870.

14 T. K. Dey, S. Tombelli, P. Biswas, A. Giannetti, N. Basumallick, F. Baldini, S. Bandyopadhyay and C. Trono, *J. Lightwave Technol.*, 2021, **39**, 4006–4012.
15 K. Sadani, P. Nag, X. Y. Thian and S. Mukherji, *Biosens. Bioelectron.: X*, 2022, **12**, 100278.
16 C. Blaszykowski, S. Sheikh and M. Thompson, *Biomater. Sci.*, 2015, **3**, 1335–1370.
17 E. Van Andel, S. C. Lange, S. P. Pujari, E. J. Tijhaar, M. M. J. Smulders, H. F. J. Savelkoul and H. Zuilhof, *Langmuir*, 2019, **35**, 1181–1191.
18 I. Víšová, M. Houska and H. Vaisocherová-Lísalová, *Analyst*, 2022, **147**, 2597–2614.
19 O. Azzaroni, *J. Polym. Sci., Part A: Polym. Chem.*, 2012, **50**, 3225–3258.
20 J. Anthi, V. Kolivoška, B. Holubová and H. Vaisocherová-Lísalová, *Biomater. Sci.*, 2021, **9**, 7379–7391.
21 X. Xu, Y. Chang, Y. Gong, Y. Zhang, Y. Yu, H. Peng and C. Fu, *ACS Appl. Polym. Mater.*, 2024, **6**, 1–27.
22 S. T. Milner, *Science*, 1991, **251**, 905–914.
23 W. J. Brittain and S. Minko, *J. Polym. Sci., Part A: Polym. Chem.*, 2007, **45**, 3505–3512.
24 M. Forinová, A. Pilipenco, N. S. Lynn, R. Obořilová, H. Šimečková, M. Vrabcová, M. Spasovová, R. Jack, P. Horák, M. Houska, P. Skládal, P. Šedivák, Z. Farka and H. Vaisocherová-Lísalová, *Food Control*, 2024, **165**, 110695.
25 M. J. Russo, M. Han, P. E. Desroches, C. S. Manasa, J. Dennaoui, A. F. Quigley, R. M. I. Kapsa, S. E. Moulton, R. M. Guijt, G. W. Greene and S. M. Silva, *ACS Sens.*, 2021, **6**, 1482–1507.
26 Q. Li, C. Wen, J. Yang, X. Zhou, Y. Zhu, J. Zheng, G. Cheng, J. Bai, T. Xu, J. Ji, S. Jiang, L. Zhang and P. Zhang, *Chem. Rev.*, 2022, **122**, 17073–17154.
27 M. Vrabcová, M. Spasovová, M. Houska, K. Mrkvová, N. S. Lynn, L. Fekete, O. Romanyuk, A. Dejneka and H. Vaisocherová-Lísalová, *Prog. Org. Coat.*, 2024, **188**, 108187.
28 M. Vrabcová, M. Houska, M. Spasovová, M. Forinová, A. Pilipenco, I. Matoušová Víšová, K. Mrkvová and H. Vaisocherová-Lísalová, *Effects of storage on stability and performance of carboxybetaine-based polymer brushes*, SPIE, 2024.
29 R. Hasler, I. Víšová, M. Vrabcová, M. Houska, M. Spasovová, H. Vaisocherová-Lísalová and J. Dostálek, *Biophotonics in Point-of-Care II*, Strasbourg, France, 2022.
30 J. O. Zoppe, N. C. Ataman, P. Mocny, J. Wang, J. Moraes and H. A. Klok, *Chem. Rev.*, 2017, **117**, 1105–1318.
31 M. Forinová, A. Pilipenco, I. Víšová, N. S. Lynn Jr., J. Dostálek, H. Mašková, V. Hönig, M. Palus, M. Selinger, P. Kočová, F. Dyčka, J. Štěrba, M. Houska, M. Vrabcová, P. Horák, J. Anthi, C.-P. Tung, C.-M. Yu, C.-Y. Chen, Y.-C. Huang, P.-H. Tsai, S.-Y. Lin, H.-J. Hsu, A.-S. Yang, A. Dejneka and H. Vaisocherová-Lísalová, *ACS Appl. Mater. Interfaces*, 2021, **13**, 60612–60624.
32 F. Chiavaioli, D. Santano Rivero, I. Del Villar, A. B. Socorro-Leránoz, X. Zhang, K. Li, E. Santamaría, J. Fernández-Irigoyen, F. Baldini, D. L. A. van den Hove, L. Shi, W. Bi, T. Guo, A. Giannetti and I. R. Matias, *Adv. Photonics Res.*, 2022, **3**, 2200044.
33 I. Víšová, M. Vrabcová, M. Forinová, Y. Zhigunová, V. Mironov, M. Houska, E. Bittrich, K.-J. Eichhorn, H. Hashim, P. Schovánek, A. Dejneka and H. Vaisocherová-Lísalová, *Langmuir*, 2020, **36**, 8485–8493.
34 A. Pilipenco, M. Forinová, H. Mašková, V. Hönig, M. Palus, N. S. Lynn Jr., I. Víšová, M. Vrabcová, M. Houska, J. Anthi, M. Spasovová, J. Mustacová, J. Štěrba, J. Dostálek, C.-P. Tung, A.-S. Yang, R. Jack, A. Dejneka, J. Hajdu and H. Vaisocherová-Lísalová, *J. Travel Med.*, 2023, **taad065**, 1–10.
35 P. Pilla, C. Trono, F. Baldini, F. Chiavaioli, M. Giordano and A. Cusano, *Opt. Lett.*, 2012, **37**, 4152–4154.
36 R. A. Dudley, P. Edwards, R. P. Ekins, D. J. Finney, I. G. McKenzie, G. M. Raab, D. Rodbard and R. P. Rodgers, *Clin. Chem.*, 1985, **31**, 1264–1271.
37 F. Chiavaioli, C. Trono, A. Giannetti, M. Brenci and F. Baldini, *J. Biophotonics*, 2014, **7**, 312–322.
38 F. Chiavaioli, P. Zubiate, I. Del Villar, C. R. Zamarreño, A. Giannetti, S. Tombelli, C. Trono, F. J. Arregui, I. R. Matias and F. Baldini, *ACS Sens.*, 2018, **3**, 936–943.

